Evidence for steady fault-accommodated strain in the High Himalaya: progressive fault rotation of the southern Tibet detachment system in NW Bhutan

G. WIESMAYR[1], M. A. EDWARDS[1,2], M. MEYER[1], W. S. F. KIDD[3], D. LEBER[1], H. HÄUSLER[1] & D. WANGDA[4]

[1] *Institut für Geologie, Universität Wien, Austria (e-mail: medwards@gmx.net)*
[2] *Previous address: Asian Tectonics Research Unit, Institut für Geologie, TU-Bergakademie Freiberg, Germany*
[3] *Department of Geological Sciences, State University of New York at Albany, Albany NY 12222, USA*
[4] *Geological Survey of Bhutan, Ministry of Trade and Industry, Thimphu, Bhutan*

Abstract: We present fault analyses from the exhumed middle crustal slab of the High Himalaya in eastern Lunana in NW Bhutan. Fault planes from within two-mica, tourmaline-bearing leucogranites, leucogranitic rocks and migmatites indicate a complex brittle fault pattern with two distinct fault groups. A first group of faults (D_1) characterized by chlorite, quartz and tourmaline slickenfibres is mainly defined by steeply SSE-dipping oblique-slip normal faults, and by shallowly NNW-dipping normal faults. A second, younger group of faults (D_2) characterized by cataclasis products comprises strike-slip faults displaying conjugate patterns and E- and W-dipping conjugate normal faults, all which indicate E–W extension. Cross-cutting relationships amongst the D_1 fault group demonstrate that progressively steeper members of the fault group become younger within the NNW-dipping faults and become older within the SSE-dipping faults. These are all post-dated by the D_2 fault group. The D_1 fault group indicates that the slab experienced ongoing NNW–SSE extension (i.e. flow) via brittle fault accommodation, contemporaneous with fault rotation. This may reflect rotation of the entire upper orogen due to movement over deeply located major ramp structures formed by out-of-sequence thrusting (Kakhtang Thrust) within the High Himalayan Slab of the Bhutan Himalaya.

The evolution of deformation accommodation processes in exhuming middle crust within mountain belts spans a history from the onset of orogenesis, through deep burial and exhumation, to final exposure and quiescence. Processes range from true high temperature intracrystalline plasticity through the poorly-understood realm or 'boundary' of frictional–viscous creep, to wholesale brittle and neotectonic processes. In this short contribution, we examine an area of relatively rapid orogenic convergence and exhumation; the eastern Himalaya. We examine the role of brittle processes in the upper part of the exhuming middle crust as part of the orogenic wedge. Here we find evidence for later-stage exhumation in the form of continued deformation accommodated by dense brittle fault networks.

Background

The Himalayan mountain belt is the Earth's largest and arguably most spectacular example of continent–continent collision. The arc is over 2000 km in length and represents the accommodation of convergence since India first collided with Asia at *c.* 65 to 55 Ma (e.g. Patriat & Achache 1984; Rowley 1998). Rates of shortening and exhumation of the Himalayan orogen are relatively rapid; present day convergence is *c.* 1–2 cm a^{-1} (Bilham *et al.* 1997) and probably has been in this range at least since the late Pliocene (Powers *et al.* 1998). Younger denudation of the Himalaya is on the order of 1 km Ma^{-1} (Einsele *et al.* 1996), and exhumation rates over the last 10 Ma are as high as 5 mm a^{-1} (Schneider *et al.* 1999). Taken together, these data imply that orogenic strain rates in the Himalaya are relatively rapid. This has relevance for our study of brittle-mechanism continued deformation of the exhuming middle crust in the High Himalaya.

Since collision began, several hundred kilometres of India have been subducted or underthrust beneath Tibet to depth of 10s to possibly greater than 100 km (e.g. Hauck *et al.* 1998; Owens & Zandt 1997; Guillot *et al.* 1997; O'Brien *et al.* 2001). This is, for the most part, expressed within rocks of amphibolite to lower granulite

From: DE MEER, S., DRURY, M. R., DE BRESSER, J. H. P. & PENNOCK, G. M. (eds) 2002. *Deformation Mechanisms, Rheology and Tectonics: Current Status and Future Perspectives.* Geological Society, London, Special Publications, **200**, 371–386. 0305-8719/02/$15

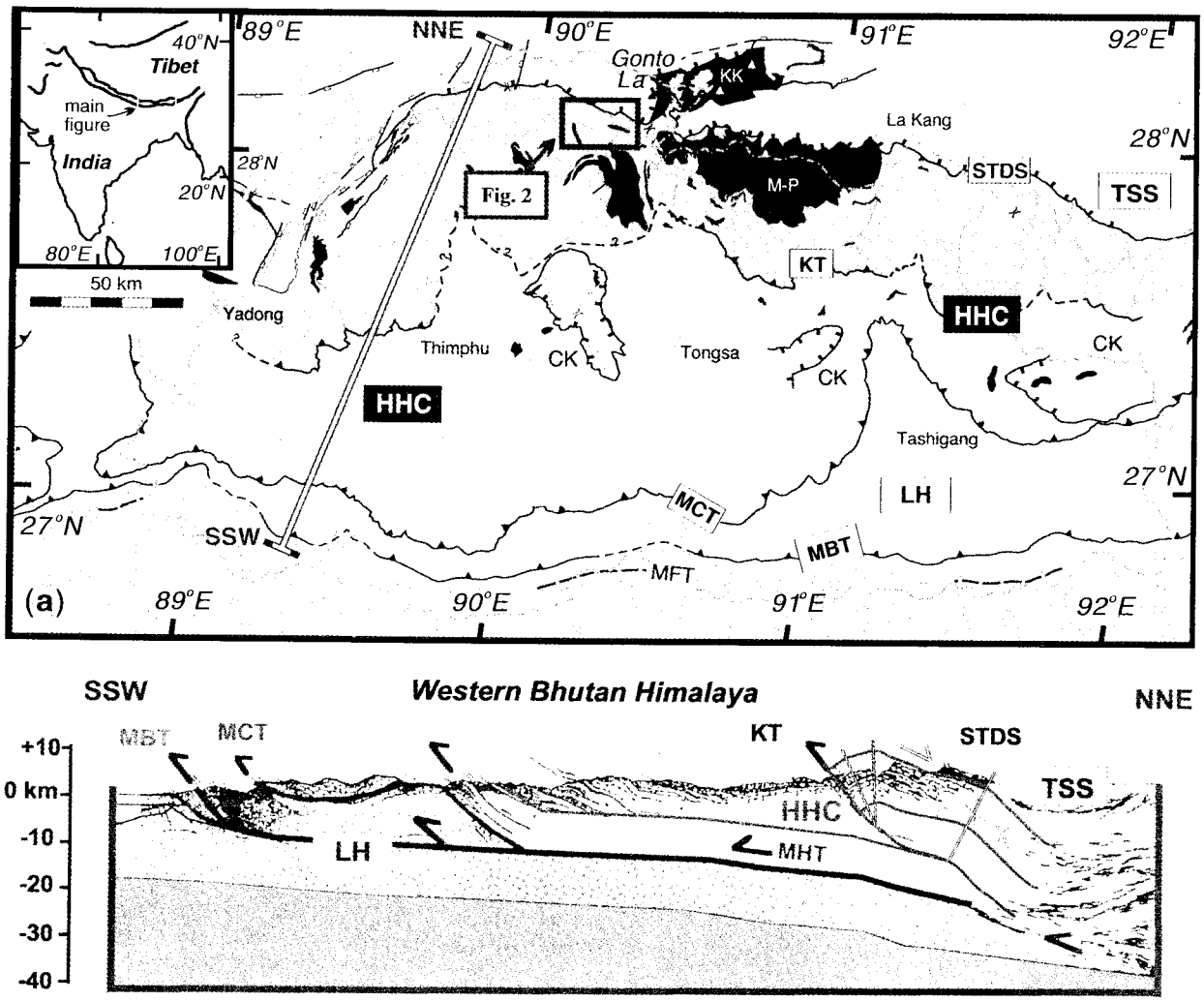

Fig. 1. (**a**) Overview geological map of Bhutan (after Gansser 1983; Edwards *et al.* 1999; Grujic *et al.* 2002. NNE–SSW is line of section shown in (**b**). Major structures: MFT, Main Frontal Thrust; MBT, Main Boundary Thrust; MCT, Main Central Thrust; CK, Klippe of Chekka Series; KT, Kakthang Thrust; STDS, Southern Tibet Detachment System. Main litho-units: LH, Lesser Himalaya; HHC, Higher Himalayan Crystalline; TSS, Tethyan Sedimentary Sequence; black shading, big Himalayan leucogranites: KK, Khula Kangri Pluton, MP, Monlakarchung-Pasalum Pluton. Other names are towns/villages. Inset shows location of main figure within Himalayan orogen. (**b**) Crustal-scale cross-section through western Bhutan Himalaya incorporating geological data from Gansser (1964) fit to interpreted reflection seismic data of Hauck *et al.* (1998). Additional interpretive crustal-scale frontal ramp and fault bend folding related to out-of-sequence thrusting on Kakhtang Thrust is proposed (see discussion).

facies that form a 5–40 km thick crystalline slab or wedge, known as the High Himalayan Crystalline (HHC: Fig. 1a and b). This wedge is bound below and above by two major tectonic discontinuities: the Main Central Thrust (MCT) and the Southern Tibet Detachment System (STDS), respectively. The MCT zone represents a several kilometer thick zone of high-strain rocks associated with an inverted metamorphic field gradient (see Grasemann & Vannay 1999 for a comprehensive review). The STDS is a system of gently N-dipping normal fault zones which typically juxtapose greenschist grade rocks over upper amphibolite to granulite facies rocks (e.g. Burg *et al.* 1983; Edwards *et al.* 1996).

The HHC in the Bhutan High Himalaya (Fig. 1) has a notably greater structural thickness than to the west in Sikkim and Nepal (Gansser 1983). This is associated with a major out-of-sequence thrust (the Kakhtang Thrust: Grujic *et al.* 1996), and is probably related to the multi-stage history of the STDS in this area (Edwards *et al.* 1996) and to the curiously young (Late Miocene) plutonism (Edwards & Harrison 1997). The major fabric of the HHC in the Bhutan High Himalaya is defined by foliation in metapelites, migmatites and high strain

zones, and is for the most part gently N-dipping. Locally, however, the HHC is domed, and gently antiformally folded to S-dipping.

Eastern Lunana

The data we report here are from the eastern Lunana area near the Tibetan frontier (Fig. 2). The area affords striking topography and full outcrop when not obscured by glaciers and Quaternary deposits. Our measurements are from the HHC of the STDS zone immediately below the Tethyan sequences in the footwall of the (southward projection of the) Gonto La detachment. The Gonto La detachment is the name given to the main low-angle normal fault of the STDS from the nearby Khula Kangri area. Southward projection of the most southerly exposure ('detachment' in Fig. 2a) shows that it is well above the present erosion surface (Fig. 2b; cf. Fig. 4 of Edwards *et al.* 1999). Overwhelmingly, the rocks present in the eastern Lunana area are two-mica, tourmaline-bearing leucogranites intruding leucogranitic and migmatitic host rocks; metapelites are conspicuous by their absence. The effects of plutonism and associated high-temperature deformation at very low relative viscosities have led to an abundance of chaotically-textured rocks made up of the interaction of intrusive bodies and migmatitic hosts. This has, almost everywhere, obscured any pre-existing foliation or planar-type regular fabric in the migmatites and orthogneisses.

Post-dating this plutonism and low viscosity deformation is a dense network of faults, the object of our study (Fig. 3). Exposed portions of the majority of fault surfaces are a few to

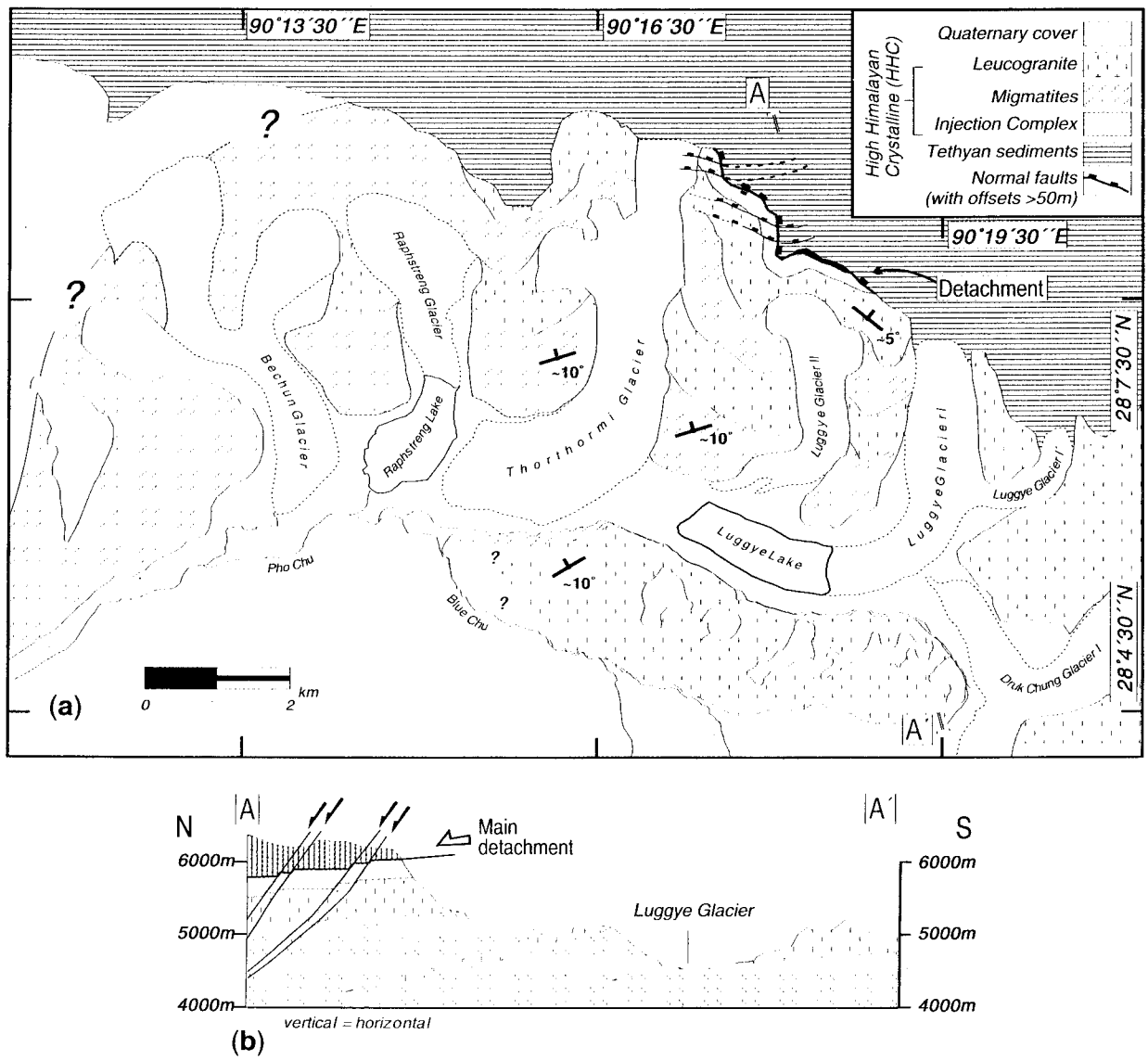

Fig. 2. Geological map (**a**) and cross-section (**b**) for eastern Lunana (after Gansser 1983; Wiesmayr, unpublished data). Legend in (**b**) as for (**a**). Map interpolated from processed remote satellite (IRS-1D) data.

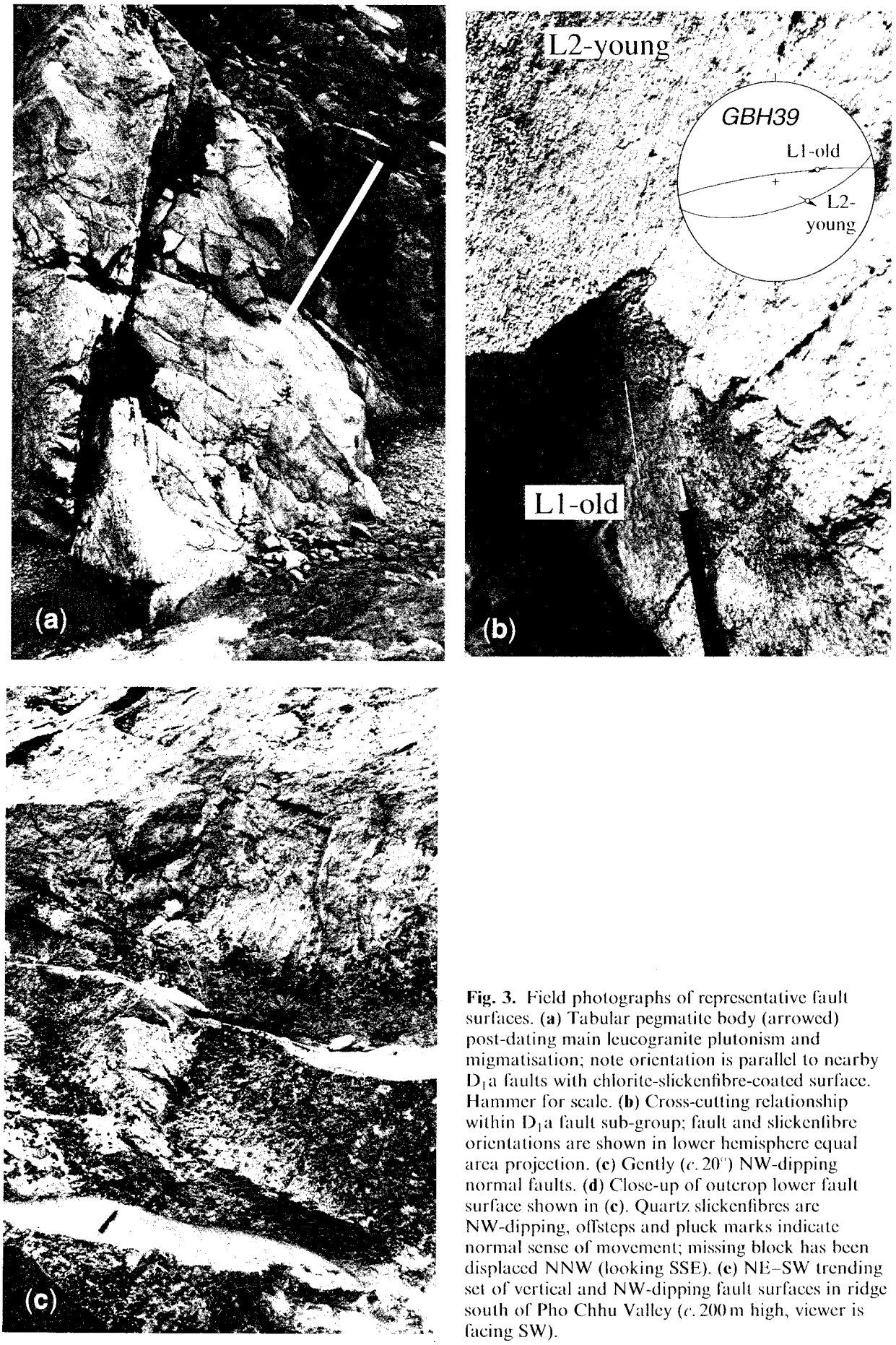

Fig. 3. Field photographs of representative fault surfaces. (**a**) Tabular pegmatite body (arrowed) post-dating main leucogranite plutonism and migmatisation; note orientation is parallel to nearby D_1a faults with chlorite-slickenfibre-coated surface. Hammer for scale. (**b**) Cross-cutting relationship within D_1a fault sub-group; fault and slickenfibre orientations are shown in lower hemisphere equal area projection. (**c**) Gently (*c.* 20°) NW-dipping normal faults. (**d**) Close-up of outcrop lower fault surface shown in (**c**). Quartz slickenfibres are NW-dipping, offsteps and pluck marks indicate normal sense of movement; missing block has been displaced NNW (looking SSE). (**e**) NE–SW trending set of vertical and NW-dipping fault surfaces in ridge south of Pho Chhu Valley (*c.* 200 m high, viewer is facing SW).

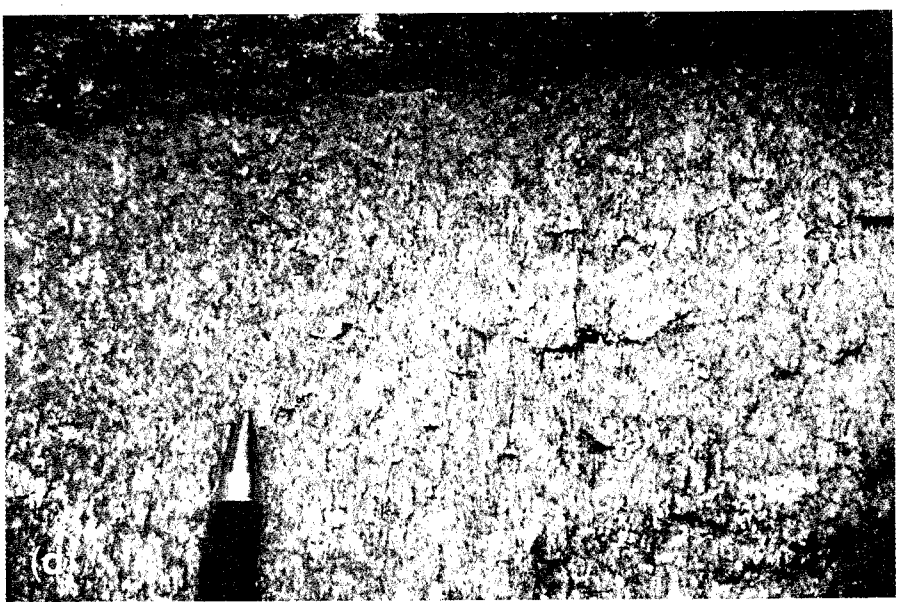

tens of metres in length, overall well-developed, and essentially planar. Faults that are present within the south wall of the Table Mountain chain in Lunana are several hundreds of metres in exposure. Surfaces are typically either sites for mineralization (tourmaline, chlorite and quartz expressed as slickenfibres) or cataclasis (various types of gouge, crush and damage zones). Some very young faults are hosts for soft sediment dyke infill. It is noteworthy that the faults do not splay, sole or diminish into, nor are they strained along with, and nor do they provide pathways for, the magmatic material that is their crystalline host rock. Locally, pegmatite bodies (all of which post-date the main leucogranite plutonism and migmatization) are found in orientations parallel to faults (Fig. 3a). The various 'low temperature' mineral deposition upon fault surfaces, and the presence of pegmatites are evidence for young fluid flow. The widespread occurrence of thermally elevated waters (e.g. 'hot springs') in the Bhutanese Highlands is further evidence for young fluid flow.

Fault analysis

Throughout the eastern Lunana area, we measured: fault size; fault orientation; sense of displacement(s); and 'overprinting' relationships if more than one phase of displacement was found preserved, or if one fault was observed cutting another (Fig. 3b). Faults include fractures of all sizes where displacement was recognisable. Fault size was qualitatively assessed from lateral extent of the displacement surface. Sense of displacement criteria include: growth direction

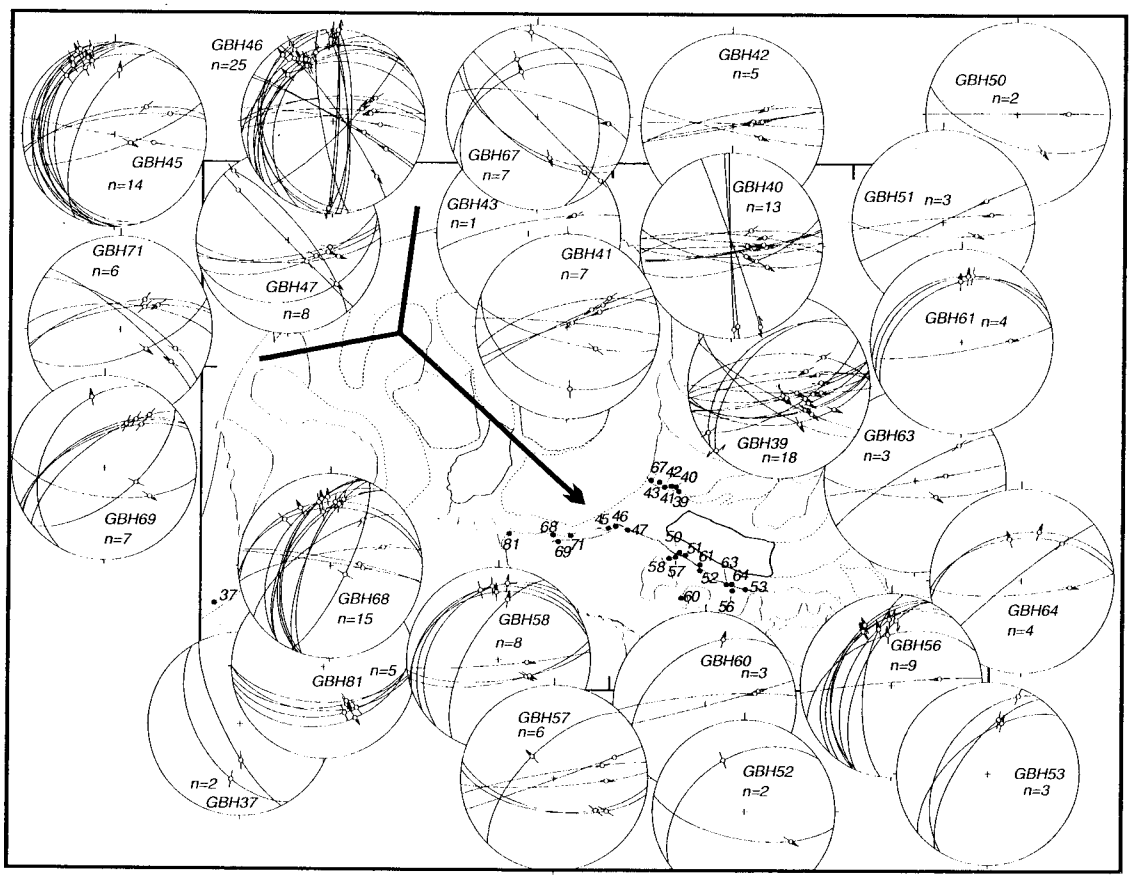
GBH46
n=25
GBH45
n=14
GBH71
n=6
GBH69
n=7
GBH47
n=8
GBH67
n=7
GBH43
n=1
GBH41
n=7
GBH42
n=5
GBH40
n=13
GBH50
n=2
GBH51 n=3
GBH61 n=4
GBH39
n=18
GBH63
n=3
GBH64
n=4
GBH56
n=9
GBH60
n=3
GBH52
n=2
GBH53
n=3
GBH57
n=6
GBH58
n=8
GBH68
n=15
GBH81 n=5
n=2
GBH37
37
67 42 40
43 41 39
68
45 46
47
50
81
69 71
58 57
51 61
52 64
63
53
60
56

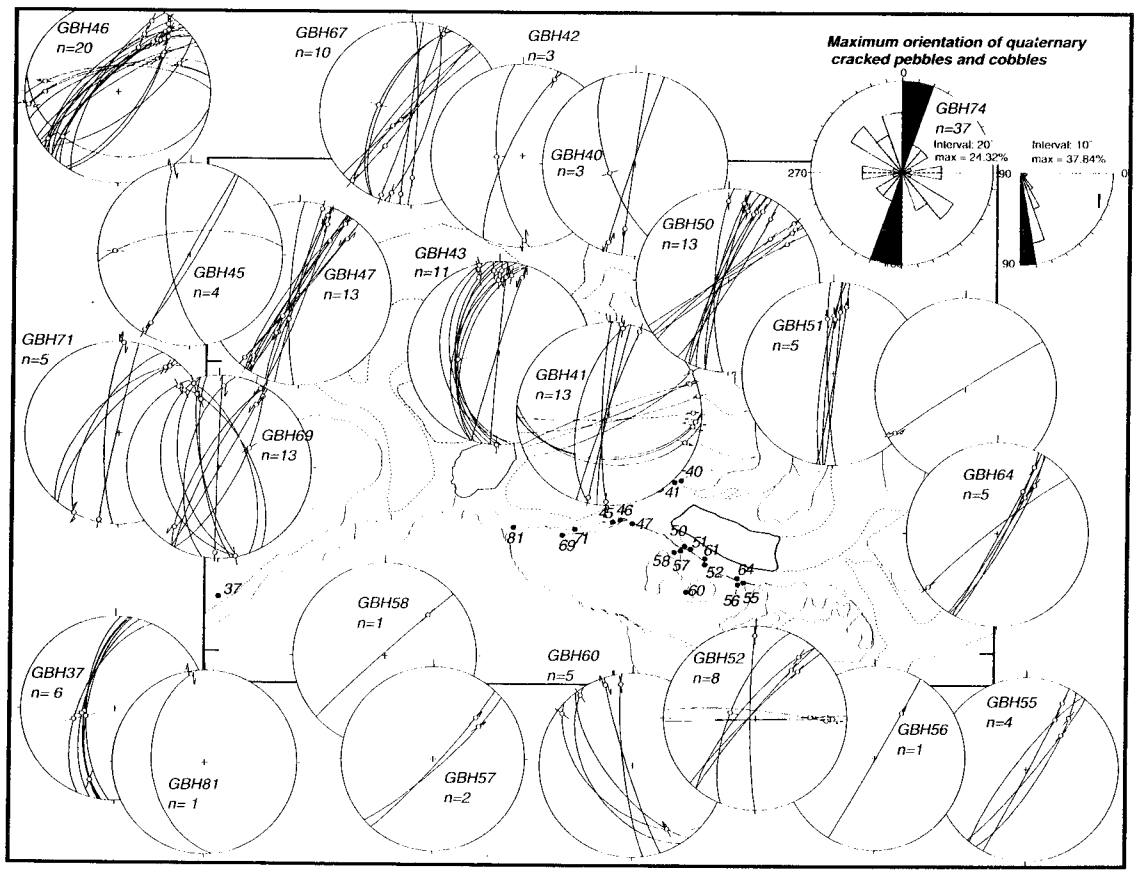
Maximum orientation of quaternary cracked pebbles and cobbles
GBH74
n=37
Interval: 20°
max = 24.32%
Interval: 10°
max = 37.84%
0
90
270
GBH46
n=20
GBH67
n=10
GBH42
n=3
GBH40
n=3
GBH50
n=13
GBH45
n=4
GBH47
n=13
GBH43
n=11
GBH71
n=5
GBH69
n=13
GBH41
n=13
GBH51
n=5
GBH64
n=5
GBH58
n=1
GBH37
n= 6
GBH81
n= 1
GBH60
n=5
GBH57
n=2
GBH52
n=8
GBH56
n=1
GBH55
n=4
37
40
41
45 46
47
50
81
69 71
58 57
51 61
52 64
60
56 55

of mineral fibers (typically slickenfibres composed of tourmaline, chlorite or quartz: Figs 3c and d); polarity of stylolites; steps or pluck marks on the fault surface; Riedel shears; and offset or aligned grains in gouge (Hancock 1985; Petit 1987).

In the field, it became apparent that faults incorporated either mineralization or cataclasis products (including soft sedimentary dyking) but nowhere were both found together. Moreover, in about fifteen instances mineralization faults were cross-cut by cataclasis product faults, but nowhere was the opposite relationship found. The relative chronology provided by this cross-cutting relationship indicates the two fault groups were generated by different events separated in time. Additionally, it is likely that the mineralization occurred at deeper crustal levels than the cataclasis, and this is consistent with the generation of the cataclasis product faults being later than the mineralization faults in the history of the steadily exhuming upper portion of the HHC. Based upon this interpretation of two separate events, we term the mineralization and cataclasis faults D_1 and D_2 respectively.

For each field locality, the fault data that we have discriminated into our D_1 and D_2 groups are displayed on Figs 4a and b, respectively. In the following section we attempt to test the robustness of this fault group discrimination.

Palaeostress and palaeostrain calculation attempts

Overall deformation has been assumed to be coaxial and offset along the faults is relatively small with respect to the spacing of faults. In this case, strain axes should coincide with stress axes. Therefore, we used kinematic as well as dynamic calculations of the stress tensor to crash test our fault group discrimination (Fig. 5). We used the numerical-dynamic analysis (NDA) Method (Spang 1972; Sperner 1996), the P–T-axes Method (Turner 1953), the Direct Inversion Method (Angelier & Goguel 1979; Sperner *et al.* 1993) and the Dihedra Method (Angelier & Mechler 1977).

There are significant limitations in using palaeostress techniques in rocks such as granites, migmatites and gneisses where there is no originally horizontal datum such as bedding. In such lithologies there is no operation to separate faults which pre- and post-date folding/tilting or rotation, in contrast to layered sedimentary rocks (e.g. Sperner *et al.* 1993). Despite these caveats, applying a palaeostress calculation can provide an identification of fault groups that were all formed under similar regimes.

We initially used non-discriminated fault data (i.e. D_1 plus D_2) from six field localities (GBH 40, 41, 46, 47, 49 & 71) whose data densities are large enough to be statistically valid for the calculation concerned (Fig. 5). In all cases, there is a striking inconsistency amongst the six localities. Moreover, the dramatic differences between the results of the four methods for each given locality provides further indication of the incompatibility of the D_1 group with the D_2 group. Note that for the P/T-axes Method and the Dihedra Method, the results are shown numerically, but not graphically. Applying each of the methods to D_1 alone and D_2 alone was more successful: D_2 fault data gave consistent results amongst the outcrops and amongst the four methods for the total summed D_2 data (D_2_all). We feel confident that D_2 is a real discrete event and that the grouping of the cataclasis product faults into a single 'event' is justified. D_1 however did not provide consistent results, neither summed nor as separate field localities, despite the visually elegant distribution of the total summed D_1 data (compare goodness of visual grouping of both D_1 _all and D_2_all with the entire D_1 plus D_2 dataset in the lower part of Fig. 5). Despite this, there are a number of key relationships within the D_1 fault group that can explain the apparent complexity.

D_1 faults

Within the investigated area, the faults that belong to D_1 form a dense network of fractures on the outcrop scale, typically displaying conspicuous black chlorite-slickenfibres and

Fig. 4. Brittle fault data measurements for each field locality. Circles are lower-hemisphere equal area projections with measured fault plane data (see text). Great circles are fault planes with accompanying lineations shown as poles and slip directions as lines. Slip direction indicated by arrow head (high confidence) or no arrow head (low confidence). GBH*x* corresponds to numbered black dot on map (field locality). *n* is number of data. Outlines of glaciers and grey shades are to allow easier cross-referencing with Fig. 2, and do not denote specific lithologies (also see Fig. 2 for lats/longs etc). **(a)** D_1 fault group (NNW–SSE extension). **(b)** D_2 fault group (conjugate strike-slip sets and E–W dipping conjugate normal faults indicating younger E–W extension), including rose diagram illustrating orientation trends of cracks in Quaternary morainal cobbles and pebbles.

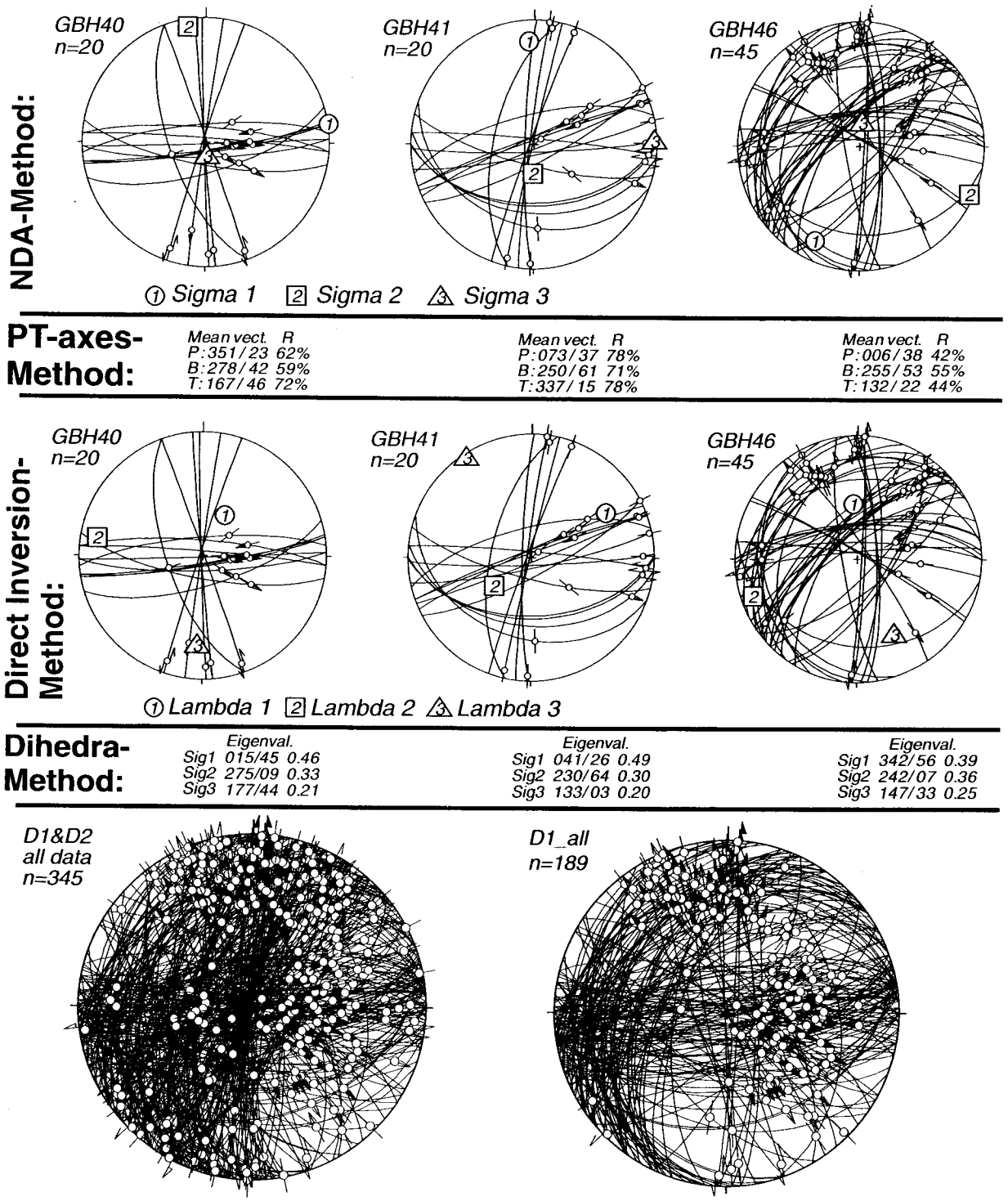

Fig. 5. Attempted palaeostress calculations using four different methods on D_1 and D_2 data sets for the six localities with densest data (upper portion). Lower portion shows total summed data for all faults (D_1 and D_2) separately. Only D_2_all gave consistent results and only these are therefore shown for all palaeostress calculation methods.

subordinate quartz-slickenfibres, both forming pronounced slickenlines. Figure 4a displays the D_1 group fault data for each field locality. Within the D_1 fault group, two sub-groups are visually apparent. Figure 6a (upper) shows a plot of all the D_1 data and a summary of the main fault orientations and lineations schematically plotted for clarity. The trends in fault orientation form two main sub-groups that we term D_1a and D_1b.

The D_1a sub-group comprises ENE–WSW trending fault planes dipping between 60–80° to the SSE, to vertical, and then to steeply NNW-dipping. Slickenside lineations vary

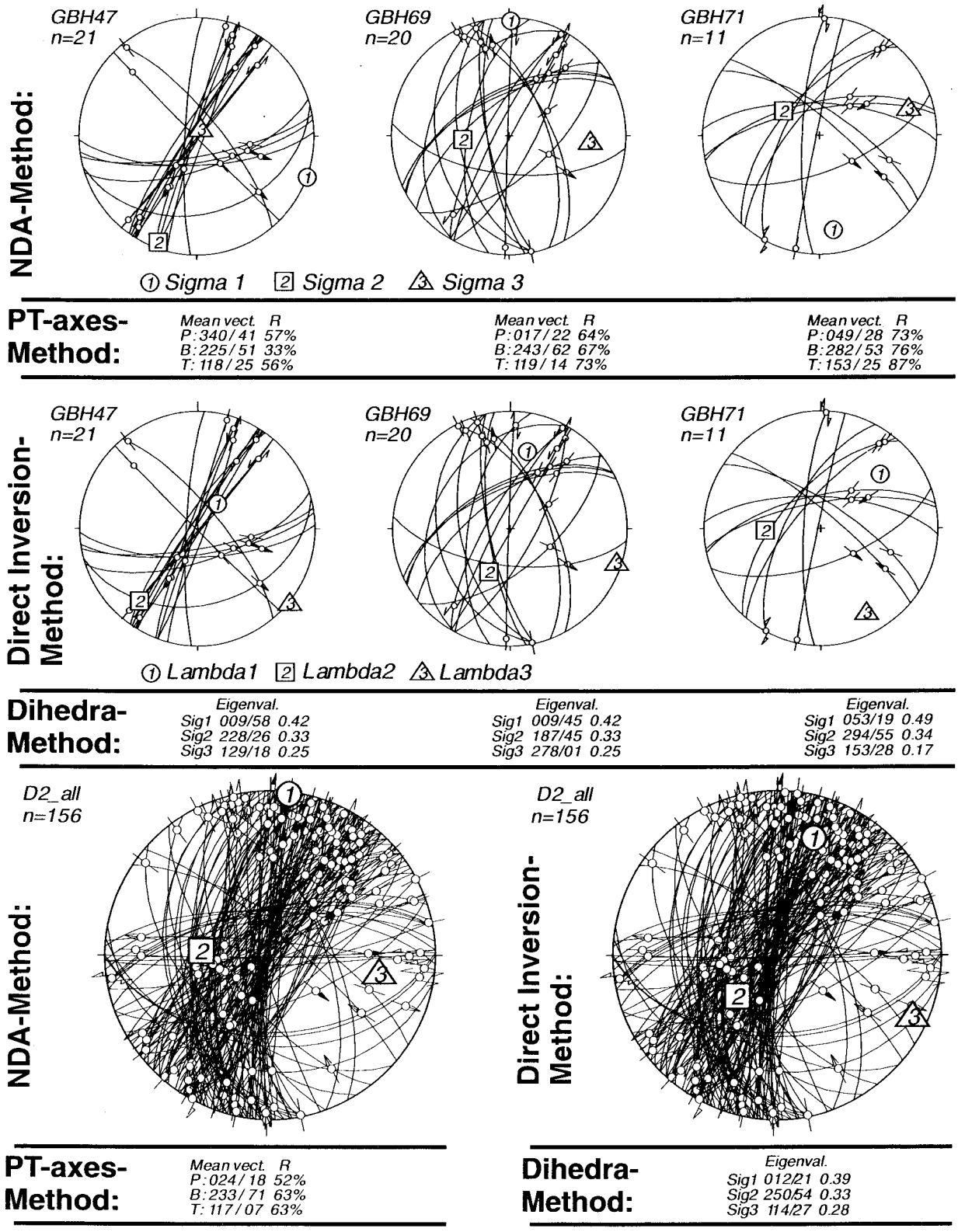

gradually with fault dip, ranging from SSE-plunging to progressively more easterly plunging with increasing fault dip. The SSE-dipping fault planes show normal and oblique slip, while for the NNW-dipping fault planes the shear sense changes to reverse displacement, thereby forming oblique thrusts (in the present orientation). Key cross-cutting fault relationships and overprinting lineations within the D_1a sub-group (Fig. 3b and Table 1) reveal that more steeply dipping faults are progressively older. The gradual change in fault orientations and displacement together with the relative chronology provided by this cross-cutting relationship is suggestive of a

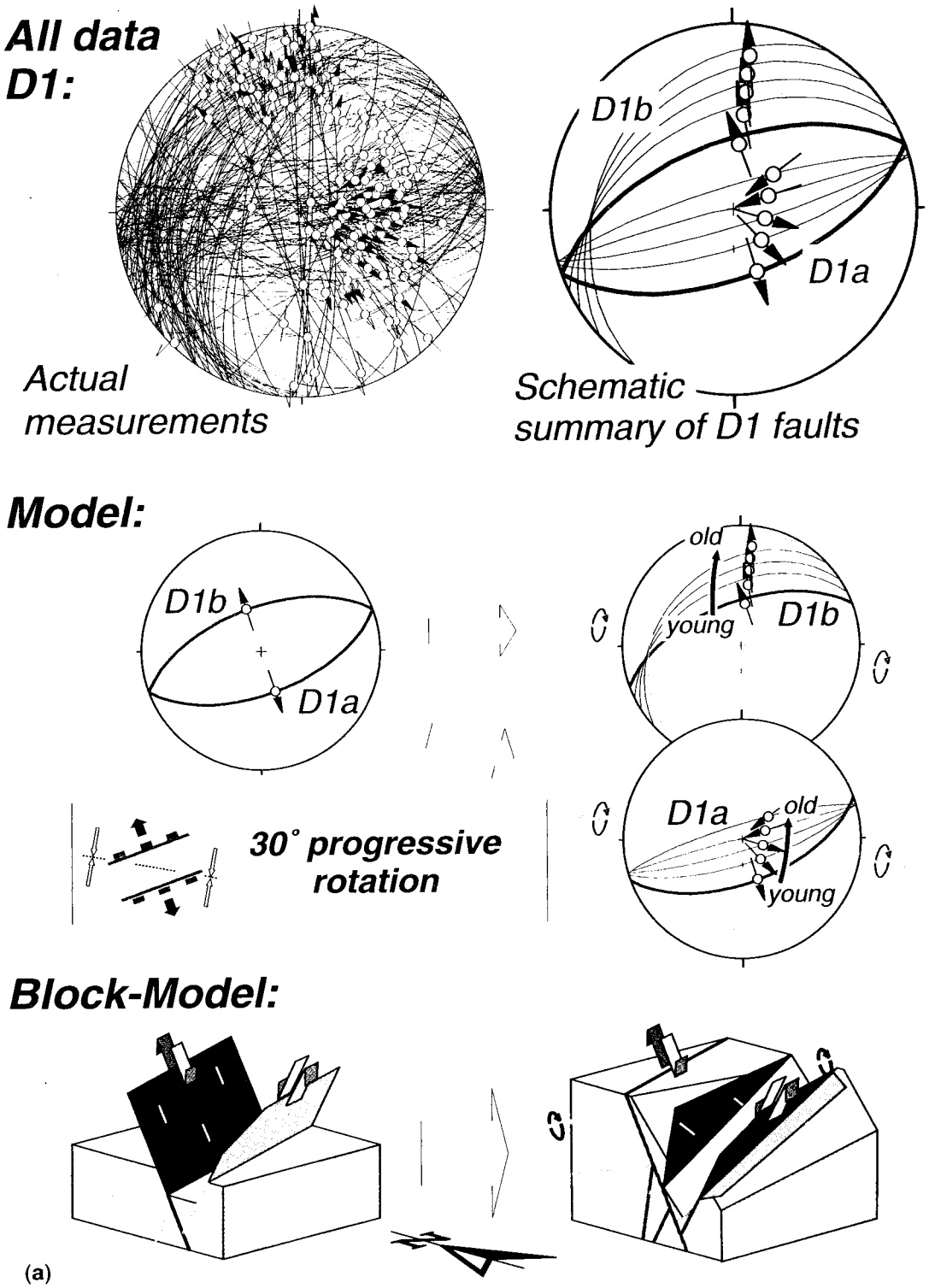

Fig. 6. **(a)** Interpretation of D_1 data and schematic model of progressive fault development. Upper portion: all D_1 data are plotted together and shown alongside a schematically displayed summary of the data illustrating how the D_1a and D_1b sub-groups are distributed. Middle portion: interpretative model of how original upright conjugate fault pairs and lineations rotate and new faults progressively form during a 30° rotation about an axis of 100/00 to give observed present-day distribution. Lower portion: 3D block model diagram of conjugate pair rotation. **(b)** General diagram of how the D_2 fault group was generated by simultaneous strike-slip and normal faulting caused by E–W extension and N–S shortening (see Fig. 5 for palaeostress results).

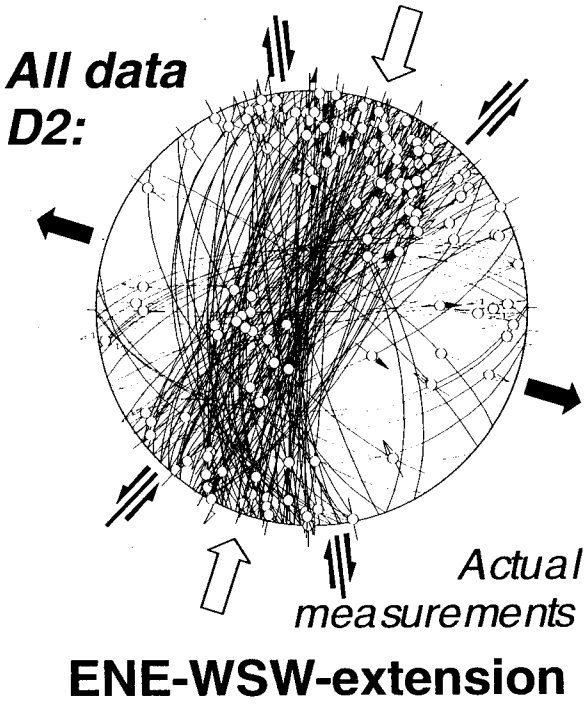

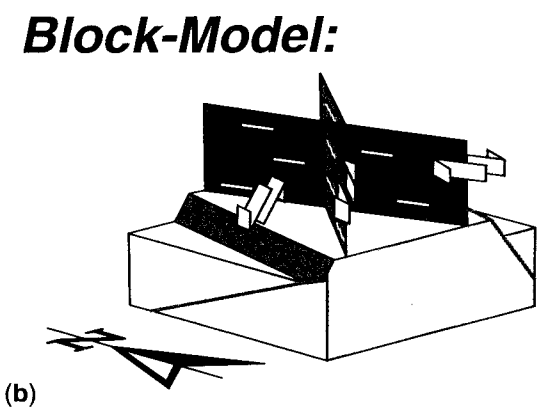

Table 1. *Relative age constraints for D_1a faults*

Outcrop	Fault	Lineation	Relative age
Examples of cross-cutting within D_1a-faults			
GBH 39	355/78	070/64	old
	164/81	157/80	young
GBH 60	355/83	080/44	old
	165/88	078/40	young
Examples of overprinting lineations on D_1a-faults			
GBH 39	181/84	112/73	young
		083/52	old
	164/81	157/80	young
		085/64	old
	165/78	150/75	young
		080/57	old
GBH 47	162/67	138/66	young
		108/52	old

rotation. In this scenario, the present steeply NNW-dipping oblique thrusts formed as SSE-dipping normal faults followed by *c.* 25–30° of rotation. In places, late stage, tourmaline-bearing pegmatitic veins and tabular bodies cross-cut the leucogranitic host gneisses. They are conspicuously parallel to the D_1a fault set (Fig. 3a). In the vicinity of the pegmatites, the faults are associated with stretched tourmaline needles that are aligned parallel to chlorite and quartz-slickenside lineations.

The D_1b sub-group consists of 60–10° NNW-dipping normal faults. Slickenside lineations change progressively from NNW- to N-plunging with decreasing fault dip. The second sub-group contains the same types of slickenfibres mineralization as the first sub-group, with chlorite and quartz linear fibres demonstrating normal sense of movement. Fault displacement is constrained by slickenfibres to be a few centimetres, reaching several tens of metres at a maximum, as shown by offset markers (cf. Fig. 2b).

D_2 faults

The D_2 group post-dates the D_1 group (see above). The faults are characterized by cataclasites formed within narrow brittle shear zones that offset D_1 faults. Figure 4b displays, for each field locality, the fault data that we have assigned to our D_2 suite. The faults mainly comprise: (1) NE–SW- to N–S-trending sinistral strike-slip faults; (2) NNW–SSE-trending dextral strike slip-faults; and (3) W-dipping normal faults (Figs 4b and 6b).

The NE–SW sinistral strike-slip faults comprise weakly to very well-developed subhorizontal lineations formed by scratching and gouging of the fault surface. The sinistral sense of displacement is also constrained by offsets of older D_1 faults. Subordinate mineralization of quartz as well as calcite occurs in fault parallel veins. The NNW–SSE dextral strike-slip faults display weak subhorizontal striations, and senses of movement are again additionally constrained by offsets of older D_1 faults. The W-, and E-dipping faults are those most commonly associated with cataclasites and are less abundant than the sinistral and dextral strike-slip faults. The overall orientation and homogeneous distribution of the faults is obvious in the remotely observed and interpolated fault traces illustrated in Fig. 7.

In addition to the cataclasis product faults of D_2 a few Quaternary or Recent features are present. Ten or so examples of steeply W-dipping, *c.* N–S trending soft-sediment fractures

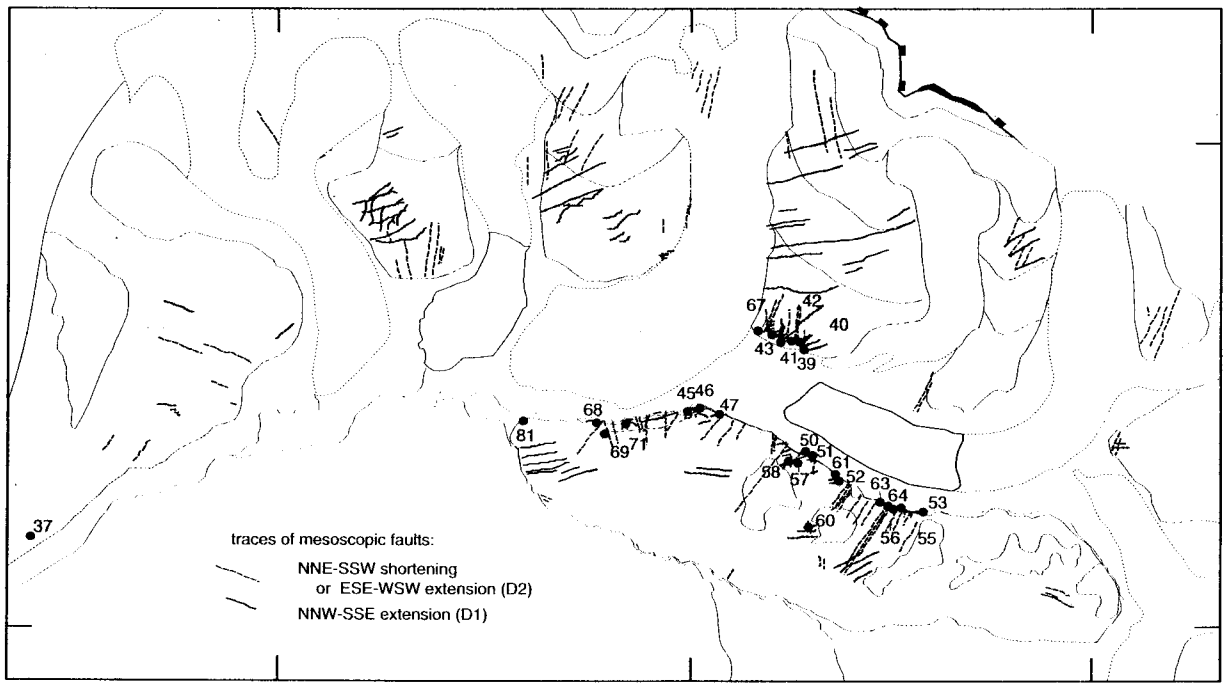

Fig. 7. Remotely sensed extrapolation of mapped and remotely observed faults throughout eastern Lunana area assisted by processed remote satellite (IRS-1D) data. Outline map from Fig. 2 employed as in Fig. 4.

infilled with sand dyke structures are present in Lunana, as well as fracture sets of partly-consolidated morainal cobbles and pebbles. Figure 4b includes frequency diagram plots of the dips and trends of the cobbles and pebbles. Based upon the orientation trends of both these features, we include them as part of the D_2 event and note that this suggests a continuation of D_2 up to the present.

Interpretation

The D_2 event appears to be straightforward. As indicated by the palaeostress calculation results, the D_2 faults are representative of a WNW–ESE extension. Figure 6b shows the basic orientation of faults forming under such a regime.

Many of the D_1 fault data show a clear progressive relationship between age and fault dip; older faults are successively more steeply dipping within the SSE-dipping D_1a fault population. Although we did not directly observe cross-cutting relationships in the D_1b sub-group, the range of fault dips is most readily interpreted as a corresponding progression of successively forming and rotating faults. This points to a straightforward scenario whereby D_1a and D_1b faults form as conjugate sets of normal faults with an acute angle of *c.* 60–40°, a result of NNW–SSE-directed extension as faults form. We infer that the faults have dynamically evolved and undergone a rotation of *c.* 25–30° about a slightly oblique, horizontal rotation axis (100/00). Simultaneously, new sets of conjugate faults have developed in the original NNW–SSE direction, leading to the scattering orientation of faults and slickenside lineations after 25–30° of finite rotation. This is schematically illustrated in the middle part of Figure 6a. This model nicely explains why steeper SSE-dipping or overturned normal faults are progressively older.

To explain the progressive rotation that we recognize in the D_1 group, we propose that the entire section of rocks examined in the field area rotated while faults were formed. Figure 8 shows a model with three time slices ($t = 3$, 2, and 1) to illustrate the approximate sequence of events that have operated in our hypothesis. Note that the three parts of the figure do not depict discrete events but snapshots of a continuous process. At the starting point ($t = 3$) the entire upper portion of the HHC slab, together with the (southern extension of the) Gonto La detachment and the overlying Tethyan rocks were dipping *c.* north at a steeper angle than is observed today. The fundamental assumption of this model is that the maximum principal stress axis ($\sigma 1$) at the Earth's surface is subvertical and $\sigma 2$ and $\sigma 3$ (the intermediate and minimum principal stress axes) are subhorizontal in the extensional regime (allowing an insignificant topographic gradient, Burchfiel & Royden 1985). Consequently, conjugate normal faults form with a *c.* 60–70° dip. At

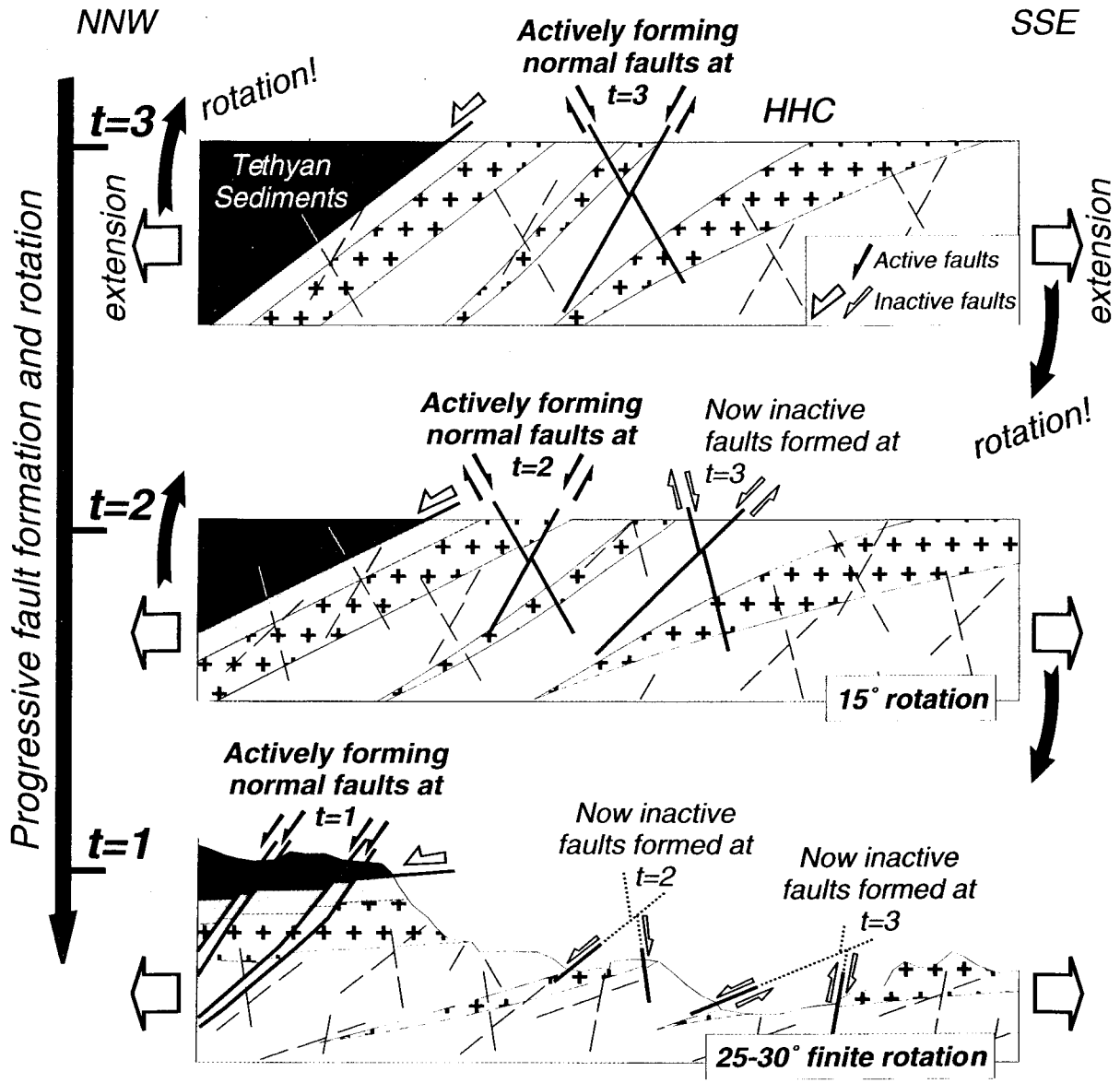

Fig. 8. Model to explain observed succession of rotated faults associated with D_1 group. Entire upper slab rotates to a total of 30°. Three stages $t = 3$, 2, and 1 are time slices of a continuous process and are not discrete events. $t = 3$: within the High Himalayan Crystalline (HHC) and the Tethyan Sediments conjugate normal faults form. $t = 2$: after 15° rotation faults formed at $t = 3$ have rotated and are now typically inactive, while new faults form. $t = 1$: after further rotation with new faults forming in the optimum orientation. Main detachment attains current *c.* dip 10° towards NNW. For clarity, only three orientations of conjugate fault pairs are selected.

$t = 3$, the upper portion of the slab is in a general state of extension (broad expansive flow). Movement along the Gonto La detachment is minimal, however, and there is no further accumulation of intra-grain strain in the granite mylonite. Only local extensional shear bands and internal minor normal faulting in the detachment hanging wall occur (see descriptions in Edwards *et al.* 1996). This point in time also marks the onset of the deformation realm where our mapped normal faults become the principal strain accommodation mechanism. After some time, $t = 2$, the slab is shown after approximately half the entire rotation (*c.* 15°). Faults formed at $t = 3$ have now rotated and are mostly inactive, and are becoming cut by newly forming faults in the optimum orientation. The final time slice shown, $t = 1$, represents the end of the rotation and present-day general geometry of the High Himalayan slab in eastern Lunana after a total of 25–30° foreland-directed finite rotation. Note that this is not $t = 0$ (the present day); the D_2 event post-dates $t = 1$. The STDS, now gently, *c.* 10° N-dipping, has repeatedly been cut by the later set of NNW-dipping D_1 normal faults.

We do not think that there has been significant slip on the faults after formation. We do not observe large fault offsets, and we speculate that cyclical fluid flux governs failure (hence faulting) to a large extent where periodic increases in hydrostatic pressure and thereby a sudden lowering of the effective stress occurs, leading to fresh faulting in favourable Mohr-Coulomb orientations being preferred rather than renewed slip on less favorably oriented pre-existing faults. Repeated cycling of fluid playing an instrumental role in rock failure is well documented from the Himalaya (Craw *et al.* 1997) and elsewhere (Fletcher 1998; Streit & Cox 2000). Note that we do not observe older faults reactivated in the opposite sense, but we do sometimes observe a normal-sense reactivation on rotated normal faults. This is consistent with the total indicated rotation for the slab being *c.* 25–30° – significantly less than the amount required to re-orient a fault into the region of opposite-sense reactivation.

Discussion

D_1 deformation

In terms of a mechanism to allow rotation of the entire thickness of the HHC in this area, we speculate that there is a crustal-scale ramp at several kilometres depth in this part of the Himalaya (Fig. 1b, originally from Gansser 1964 and Hauck *et al.* 1998). In this figure we have included the Kakhtang Thrust, a crustal structure that incorporates a frontal ramp in the main Himalayan thrust (Edwards *et al.* 1996; Grujic *et al.* 1996). This provides a mechanism for rotation of the HHC in this area. We allow fault bend folding of the entire upper slab as out-of-sequence displacement along the Kakhtang Thrust is accommodated. The progressive transport of the overthrusting slab along the Kakhtang structure results in a clear gradual rotation. It is important to note that only a small portion of the HHC is considered here: i.e. the area above the Kakhtang Thrust that is restricted to the western Bhutan High Himalaya. Moreover, we stress that this is a general suggestion to allow the upper HHC to rotate.

The three light grey crosses in Fig. 1b correspond to the fate of one conjugate fault pair initially formed on the lower ramp at three separate stages ($t = 3$, 2, and 1) during the advance of the slab as it is transported up and over the ramp of the Kakhtang Thrust. Subsequent newly forming faults are not shown. Note that the region of extension is not large. It can either be the general realm above a neutral surface of the slab travelling through the fault bend fold hinge, or a general region of extension in the upper portion of the slab synchronous with lower level contraction, as shown by wedge extrusion models for the HHC (e.g. Vannay & Grasemann 2001 and references therein).

Our suggested rotation of the entire HHC is not, we feel, unreasonable or without precedent. Edwards *et al.* (1996) discussed the likelihood of a 20–30° rotation of the Gonto La detachment based upon the presence of a cross-cutting steep normal fault (the Dzong Chu Fault) all along the northern portions of the Khula Kangri area. Other supporting evidence in the form of palaeomagnetic data has been reported from both the Spiti (NW India) and from Manaslu (Nepal), for example, where Schill *et al.* (2001, 2002) obtained data for a corresponding rotation of the upper HHC in this area. Deep seismic reflection data from Hauck *et al.* (1998) lend further support; these authors have shown evidence for large crustal scale features at depth below southern Tibet. Earthquake studies have additionally shown the occurrence of seismic slip deeper than 40 km in this area (Ekstrom 1987).

Our model is inconsistent with a channel–flow model to explain the thermotectonic evolution of the HHC (Grujic *et al.* 2002). Such a model requires that the present-day dips, and thus angles between, the MHT and the STDS have remained unchanged since times of high-temperature ductile flow of the HHC slab.

D_2 deformation

The E–W extension of D_2 is consistent with widespread observations throughout southern Tibet and the Himalaya of young E–W expansion (e.g., the graben systems of Armijo *et al.* 1986). It has been debated, however, whether E–W extension is contemporaneous with, or post-dates, the N–S extension associated with the STDS. Our data support the latter view or, at a minimum, require that the history of E–W extension in southern Tibet is protracted.

Conclusion

Fault surface slip data from the High Himalaya in eastern Lunana indicate two deformation products. A NNW-directed extension of D_1 is indicated by steeply SSE-dipping oblique-slip, and shallowly NNW-dipping, normal faults, while a (younger) E–W extension of D_2 is

indicated by E-, and W-dipping conjugate pattern strike-slip faults. Progressive cross-cutting relationships amongst the D_1 fault group indicate a rotation of the local upper Himalaya. We speculate that this is due to a crustal-scale ramp and extension in the upper part of the HHC related to late reverse faulting along the Kakhtang Thrust. The D_2 E–W extension is considered to be part of the extension ubiquitous throughout southern Tibet.

The work of the Austrian party was funded within the Austrian–Bhutanese Glacial Lake Outburst Flood (GLOF) Mitigation Project, funded by the Austrian Federal Ministry of Foreign Affairs. We thank all the members of the Bhutan expedition of the University of Vienna, the University of Agricultural Sciences, Vienna and the Geological Survey of Bhutan for assistance and open discussion of ideas and data. Part of the writing was completed while G. Wiesmayr was visiting Freiberg as a DAAD scholar. We are indebted to B. Grasemann for speedy assistance on several occasions and to R. Lisle and an anonymous reviewer for very constructive reviews.

References

ANGELIER, J. & GOGUEL, J. 1979. Sur une méthode simple de détermination des axes pricipaux des constraintes pour une population de failles. *Comptes Rendus de l'Academie des Sciences, Paris*, **288**, 307–310.

ANGELIER, J. & MECHLER, P. 1977. Sur une méthode graphique de recherche des constraintes principales également utilisable en tectonique et en séismologie: la methode des dièdres droits. *Bulletin de la Société Géologique de France*, **7**, 1309–1318.

ARMIJO, R., TAPPONNIER, P., MERCIER, J. L. & TONGLIN, H. 1986. Quaternary extension in southern Tibet: Field observations and tectonic implications. *Journal of Geophysical Research*, **91**, 13803–13872.

BILHAM, R., LARSON, K., FREYMÜLLER, J. & MEMBERS, P. I. 1997. GPS measurements of present-day convergence across the Nepal Himalaya. *Nature*, **386**, 61–64.

BURCHFIEL, B. C. & ROYDEN L. H. 1985. North–south extension within the convergent Himalayan region. *Geology*, **13**, 679–682.

BURG, J. P., PROUS, F., TAPPONNIER, P. & MING, C. G. 1983. Deformation phase and tectonic evolution of the Lhasa block. *Eclogae Geologicae Helveticae*, **76**, 643–665.

CRAW, D., CHAMBERLAIN, C. P., ZEITLER, P. K. & KOONS, P. O. 1997. Geochemistry of a dry steam geothermal zone formed during rapid uplift of Nanga Parbat, northern Pakistan. *Chemical Geology*, **142**, 11–22.

ECKSTROM, G. A. 1987. *A Broad Band Method of Earthquake Analysis*. PhD thesis, Harvard University.

EDWARDS, M. A. & HARRISON T. M. 1997. When did the roof collapse? Late Miocene N–S extension in the High Himalaya revealed by Th-Pb monazite dating of the Khula Kangri granite. *Geology*, **25**, 543–546.

EDWARDS, M. A., KIDD, W. S. F., LI, J., YUE, Y. & CLARK, M. 1996. Multi-stage development of the southern Tibet detachment system near Khula Kangri. New data from Gonto La. *Tectonophysics*, **260**, 1–19.

EDWARDS, M. A., PÊCHER, A., KIDD, W. S. F., BURCHFIEL, B. C. & ROYDEN, L. H. 1999. The Southern Tibet Detachment System (STDS) at Khula Kangri, Eastern Himalaya: a large area, shallow detachment stretching into Bhutan? *Journal of Geology*, **107**, 623–631.

EINSELE, G., RATSCHBACHER, L. & WETZEL, A. 1996. The Himalaya-Bengal fan denudation-accumulation system during the past 20 Ma. *Journal of Geology*, **104**, 163–184.

FLETCHER, C. 1998. Effects of pressure solution and fluid migration on initiation of shear zones and faults. *Tectonophysics*, **295**, 139–165.

GANSSER, A. 1964. *The Geology of the Himalayas*. John Wiley, London.

GANSSER, A. 1983. *Geology of the Bhutan Himalayas*. Birkhauser Verlag, Basel.

GRASEMANN, B. & VANNAY, J. C. 1999. Flow controlled inverted metamorphism in shear zones. *Journal of Structural Geology*, **21**, 743–750.

GRUJIC, D., CASEY, M., DAVIDSON, C., HOLLISTER, L. S., KÜNDIG, R., PAVLIS, T. & SCHMID, S. 1996. Ductile extrusion of the Higher Himalayan Crystalline in Bhutan: evidence from quartz microfabrics. *Tectonophysics*, **260**, 21–43.

GRUJIC, D., HOLLISTER, L. S. & PARISH, R. R. 2002. Himalayan metamorphic sequence as an orogenic channel: insight from the kingdom of Bhutan. *Earth and Planetary Science Letters*, **198**, 177–191.

GUILLOT, S., DE SIGOYER, J., LARDEAUX, J. M. & MASCLE, G. 1997. Eclogitic metasediments from the Tso Morari area (Ladakh, Himalaya): evidence for continental subduction during India-Asia convergence. *Contributions to Mineralogy and Petrology*, **128**, 197–212.

HANCOCK, P. L. 1985. Brittle microtectonics: principles and practice. *Journal of Structural Geology*, **7**, 437–457.

HAUCK, M. L., NELSON, K. D., BROWN, L. D., ZHAO, W. & ROSS, A. R. 1998. Crustal structure of the Himalayan orogen at *c.* 90° east longitude from Project INDEPTH deep reflection profiles. *Tectonics*, **17**, 481–500.

O'BRIEN, P. J., ZOTOV, N., LAW, R., KHAN, M. A. & JAN, M. Q. 2001. Coesite in Himalayan eclogite and implications for models of India-Asia collision. *Geology*, **29**, 435–438.

OWENS, T. J. & ZANDT, G. 1997. Implications of crustal property variations for models of Tibetan plateau evolution. *Nature*, **387**, 37–42.

PATRIAT, P. & ACHACHE, J. 1984. India-Eurasia collision chronology has implications for crustal shortening and driving mechanism of plates. *Nature*, **311**, 615–621.

PETIT, J. P. 1987. Criteria for the sense of movement on fault surfaces in brittle rocks. *Journal of Structural Geology*, **9**, 597–608.

POWERS, P. M., LILLIE, R. J. & YEATS, R. S. 1998. Structure and shortening of the Kangra and Dehra Dun re-entrants, Sub- Himalaya, India. *GSA Bulletin*, **110**, 1010–1027.

ROWLEY, D. B. 1998. Minimum age of initiation of collision between India and Asia north of Everest based upon the subsidence history of the Zhepure Mountain section. *Journal of Geology*, **106**, 229–235.

SCHILL, E., APPEL, E., GAUTAM, P. & DIETRICH, P. 2002. Thermo-tectonic history of the Tethyan Himalayas deduced from palaeomagnetic record of metacarbonates from central Nepal (Shiar Khola). *Journal of Asian Earth Science*, **20**, 203–210.

SCHILL, E., APPEL, E., ZEH, O., SINGH, V. K. & GAUTAM, P. 2001. Coupling of late-orogenic tectonics and secondary pyrrhotite remanences: towards a separation of different rotation processes and quantification of rotational underthrusting in the western Himalayas (N-India). *Tectonophysics*, **337**, 1–21.

SCHNEIDER, D. A., EDWARDS, M. A., KIDD, W. S. F., KHAN, A. M., SEEBER, L. & ZEITLER, P. K. 1999. Tectonics of Nanga Parbat, western Himalaya: synkinematic plutonism within the doubly vergent shear zones of a crustal-scale pop-up structure. *Geology*, **27**, 999–1002.

SPANG, J. H. 1972. Numerical method for dynamic analysis of calcite twin lamellae. *Geological Society of America Bulletin*, **83**, 467–472.

SPERNER, B. 1996. *Computer programs for the finematic analysis of brittle deformation structures and the ertiary tectonic evolution of the western Carpathians (Slovakia)*. Tübinger Geowiss, Arbeiten, A27.

SPERNER, B., RATSCHBACHER, L. & OTT, R. 1993. A Turbo Pascal program package for graphical presentation and reduced stress tensor calculation. *Computers and Geoscience*, **19**, 1361–1388.

STREIT, J. E. & COX, F. E. 2000. Asperity interactions during creep of simulated faults at hydrothermal conditions. *Geology*, **28**, 231–234.

TURNER, F. J. 1953. Nature and dynamic interpretation of deformation lamellae in calcite of three marbles. *American Journal of Science*, **251**, 276–298.

VANNAY, J. C. & GRASEMANN, B. 2001. Himalayan inverted metamorphism and syn-convergence extension as a consequence of general shear extrusion. *Geological Magazine*, **138**, 253–276.